Climate Dynamics
https://doi.org/10.1007/s00382-024-07318-8

ORIGINAL ARTICLE

Added value of EURO-CORDEX downscaling over the complex orography region of the Pyrenees

Nerea Bilbao-Barrenetxea[1,2] · María Santolaria-Otín[3] · Claas Teichmann[4] · Sérgio Henrique Faria[1,5] · María Máñez-Costa[4]

Received: 10 January 2024 / Accepted: 18 June 2024

Abstract
This study presents an assessment of the added value of downscaling utilizing Regional Climate Models (RCMs) compared to Global Climate Models (GCMs) in the high mountain region of the Pyrenees, characterized by complex topography. The EURO-CORDEX ensemble was investigated, employing a gridded high-resolution observational database as a reference. A recently proposed method is applied to quantify the performance gains or losses associated with dynamic downscaling. Our analysis focuses on calculating the added value by exploring the extremes of the Probability Density Function (PDF), spatial distribution patterns, and its relationship with elevation. Overall, our findings reveal significant improvements in the representation and general characterization of precipitation, minimum temperature, and maximum temperature in the Pyrenean region. Furthermore, RCMs demonstrate enhanced performance in capturing maximum precipitation events; however, they struggle to represent low precipitation rates, particularly in the Mediterranean area of the mountain range. Regarding temperature extremes, dynamical downscaling exhibits improvements in capturing maximum events. Nevertheless, deficiencies are observed in the RCMs' representation of minimum temperature events for both minimum and maximum temperature variables, as well as in representing near-freezing temperatures.

Keywords Regional climate models · Added value · High mountain · Pyrenees · EURO-CORDEX

1 Introduction

Regional Climate Models (RCMs), have been developed in the recent decades to address the challenge of downscaling low-resolution models (GCMs) into high-resolution information. This approach overcomes the practical limitations of employing high-resolution models on a global scale. Over the past years, RCMs have gained increasing significance, primarily due to the growing demand for high-resolution simulations to conduct impact assessment studies for climate change adaptation strategies. However, despite the advantages of these models, there are limitations that must also be taken into account (Kotlarski et al. 2014, 2015; Vautard et al. 2021)

In this scenario of the proliferation of RCMs, the Coordinated Regional climate Downscaling Experiment, CORDEX (Giorgi et al. 2009; Jones et al. 2011; Gutowski et al. 2016), was created. In particular, for the European region, more than 70 RCM simulations have currently been conducted within the framework of the EURO-CORDEX initiative. However, downscaling the information derived from GCMs is computationally very expensive. Therefore, it is a prior need to assess the added value (AV) of using RCMs against GCMs in simulating the climate system.

For this aim, previous studies have proposed different methods to compute the AV depending on multiple factors such as the variable, the region of interest and the spatial and temporal scale. Di Luca et al. (2016) proposed the potential added value metric, which delves into the increased

✉ Nerea Bilbao-Barrenetxea
nbilbao034@ikasle.ehu.eus

1 Basque Centre for Climate Change (BC3), 48940 Leioa, Spain

2 Faculty of Science and Technology, University of the Basque Country (UPV/EHU), 48940 Leioa, Spain

3 Group of Meteorology, Universitat de Barcelona (UB), 08028 Barcelona, Spain

4 Climate Service Center Germany (GERICS), Helmholtz-Zentrum Geesthacht, 20095 Hamburg, Germany

5 Basque Foundation for Science, IKERBASQUE, 48009 Bilbao, Spain

Published online: 08 July 2024

spatial-scale variability not present in the simulations at lower resolutions. This approach involves analyzing the discrepancies in high-ranking percentiles at the scale of individual grid-cells. The results showed potential added value values in regions of complex topography and short time scales, especially less than 3 h. Perkins et al. (2007) proposed a metric to measure the ability of a model to simulate the full observational distribution of a climate variable. This methodology enables us to direct our analysis towards a specific segment of the PDF, for example, its tails, making possible to study low-probability events that are not reflected in the mean. Soares and Cardoso (2018) combined the definition of AV proposed by Di Luca et al. (2016) and the definition of model skill proposed by Perkins et al. (2007) to create a new metric called DAV (Distributed Added Value) that provides a normalized measure of the added value in relation to the gain associated with downscaled simulations, comparing the PDFs of the RCMs and GCMs with observations. The results showed positive AVs for precipitation throughout the European region, specifically where convective processes are relevant, such as the Alps or Iberian Peninsula. In that line, Ciarlo et al. (2021) applies a point-by-point analysis of PDFs to spatially assess the added value of a RCM, including both a comprehensive representation of the characteristics of a variable and its geographical variation. Quantifications of the PDF-based AV indicate that higher AV values are obtained at the tails ends of the distribution for the precipitation variable.

Common outcomes are reported in the literature (Feser 2006; Prein et al. 2016; Fantini et al. 2018; Di Luca et al. 2016; Torma et al. 2015; Ciarlo et al. 2021; Qiu et al. 2020). First, the increase of AV with spatial resolution is associated with a better representation of topographic features. This results in a significant increase in AV in regions with complex topography, such as mountainous or coastal areas. Secondly, it is emphasized that there is a substantial improvement in AV even when the RCMs have been upscaled to the GCM grid. This means that the better performance of the RCM is due to a better representation of the physical processes and not to the disaggregation of the large-scale forcing. In addition, they all point out the importance of having high-quality observational data due to the impact they have when computing the AV index, especially significant in the tails of the distribution (Ciarlo et al. 2021) which makes accurate analysis limited in many regions of the globe.

The high-mountain region of the Pyrenees spans from the Cantabrian to the Mediterranean coast having a climate of both Atlantic and Mediterranean influence. It is a particularly vulnerable region to climate change with impacts on essential sectors such as water management or tourism (Amblar-Francés et al. 2020). Until present, the Pyrenees have not been considered separately when evaluating the benefits or losses of using high versus low resolution models. In this work, the assessment of AV in the Pyrenees is performed, considering the entire mountain region as the area of interest and focusing on the performance of RCMs versus GCMs.

2 Materials and methods

2.1 Data

In this study, the added value method proposed by Ciarlo et al. (2021) was applied to quantify the gain or loss representing a variable when using RCMs or GCMs in the Pyrenees region (41°N–44°N, 2.5°W–3.5°E). This metric is based on the Probability Distribution Function (PDF) of each grid point providing a spatial distribution of the added value over the study area. It combines the spatial downscaling signal described by Giorgi et al. (2009) and the spatial correlation skill mentioned in Rummukainen (2016) allowing a spatial analysis over the whole PDFs. Daily precipitation ("pr"), maximum temperature ("tmax"), and minimum temperature ("tmin") were analyzed using a high-resolution observational dataset against a set of RCMs and GCMs. Furthermore, the orography ("orog") variable from model simulations was considered to further investigate the relationship between the added valued and the elevation.

CLIMPY observational dataset covering the Pyrenees (Cuadrat et al. 2020) was used as reference with a spatial resolution of 1 km × 1 km on a daily basis covering the period 1981–2015. It is a reconstruction (Serrano-Notivoli et al. 2017) of the variables based on the information from 1343 meteorological stations located in Spain, France, and Andorra. This dataset was created in the framework of the transboundary project CLIMPY and has already been validated in different studies (Amblar-Francés et al. 2020; Lemus-Canovas and Lopez-Bustins 2021).

We evaluated the EURO-CORDEX ensemble (Jacob et al. 2014, 2020), with a total of 72 RCM simulations (Table 1) and a spatial resolution of 0.11°. These simulations cover a time period of 130 years and are available for different Representative Concentration Pathways (RCP4.5, RCP8.5, and RCP2.6). This analysis focuses on the period from 1980 to 2015. Data from 1980 to 2005 is extracted from historical simulations, while data from 2005 to 2015 comes from simulations under the RCP85 emission scenario. These simulations consist of two models, the RCM and the driver model, the GCM (with a resolution of 1.00°), forming an incomplete matrix of 12 RCMs and 8 GCMs (Fig. 1).

In this study, the data will undergo interpolation onto two rectilinear grids with resolutions of 0.11° and 1.00°, corresponding to the RCM and GCM models, respectively. Interpolation to the finer resolution (0.11°) was accomplished using the distance-weighted average remapping method

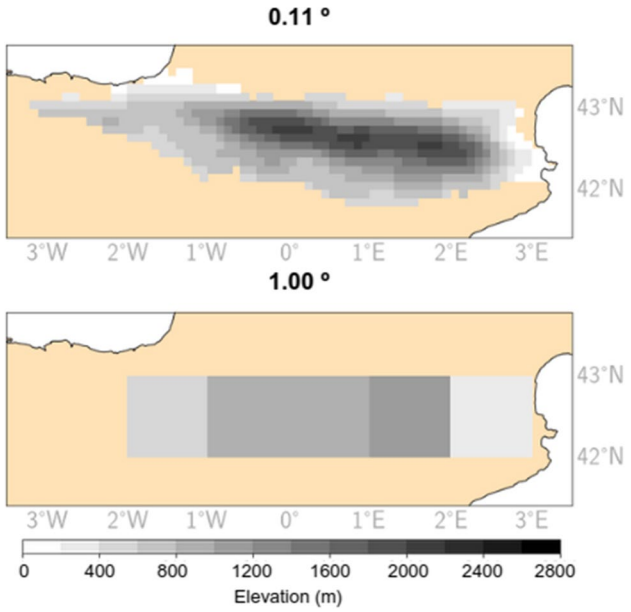

Fig. 1 Topography for the Pyrenean analysis region at the two resolutions investigated in this work: top (0.11°) and bottom (1.00°)

(Ciarlo et al. 2021; Fantini et al. 2018; Torma et al. 2015) implemented in the Climate Data Operators software (CDO, https://code.zmaw.de/projects/cdo). This method, as noted by Torma et al. (2015), yields the most consistent spatial patterns across different resolutions. Additionally, the analysis incorporates evaluation at the native resolution of the GCMs, where all data (including observations and RCMs) are upscaled to a 1.00° grid. This approach, as highlighted by Terzago et al. (2017) and Vautard et al. (2021), mitigates the impact of horizontal resolution on the performance of coarser-scale climate models. Spatial interpolation for this step utilize conservative remapping, also available within CDO.

2.2 Methodology

For each grid point the PDF of the daily events (including dry events for precipitation) were computed, over the period 1981–2015 for each variable in the observations, RCMs, and GCMs. To ensure the consistency in the bin size across all three datasets and for each variable, a bin size of 1 mm/day for the precipitation variable as in Ciarlo et al. (2021) and a 0.5 °C for the minimum and maximum temperature variables as in Perkins et al. (2007), were selected.

Then, the Relative Probability Difference (D_M) was computed following the methodology defined in Ciarlo et al. (2021) by (1), which provides information about the discrepancies that exist between the distributions of the observations and the models, whether GCM or RCM. That is, a higher (lower) value of D_M means a worse (better) performance of the model

$$D_M = \frac{\sum_{v=1}^{v_t} |(N_M - N_O)|\Delta v}{\sum_{v=1}^{v_t} (N_O \Delta v)}, \tag{1}$$

where N_M and N_O are, respectively, the number of events for the GCM or RCM and observations per bin, and Δv is the bin size of the variable. Two values for D_M, namely D_{RCM} and D_{GCM}, for the RCM and GCM simulations, respectively, were obtained.

Hence, the Added Value (AV) index is defined as the difference between both estimates of D_M as shown in (2), previously defined in Ciarlo et al. (2021). A positive (negative) AV value represents an improvement (worsening) in the results of the RCM in relation to the GCM when representing the probability distribution of the variable

$$AV = D_{GCM} - D_{RCM}. \tag{2}$$

Note that, for the exceptional case when the GCM does not simulate events for a specific bin (for instance, at the tails of the distribution, i.e., extreme values), N_{GCM} will be zero, while the value of N_O and N_{RCM} may not. In this situation, the value of D_{GCM} will always be equal to 1, while D_{RCM} could exceed this value, which significantly disturbs the AV calculation by obtaining misleading negative AV values. Hence, a conditional assumption is applied. In this scenario, if N_{GCM} is equal to zero for a particular bin, yet N_{RCM} and N_O are both non-zero, the D_{RCM} value for that bin is zero. This approach guarantees a positive contribution to the AV index in these cases. The inverse condition, namely, the cases where both N_{GCM} and N_O are non-zero while N_{RCM} equals zero, has not been considered. This omission arises from the negligible number of instances relative to the total number of events, accounting for less than 0.01%.

To shed light on the relationships between AV and elevation, the linear relationship was calculated with the Pearson correlation coefficient. A 95% level of significance, corresponding to a p value equal to 0.05 was considered and computed as follows: for a given sample with correlation coefficient r, the p-value is the probability that the absolute value of the correlation coefficient ($|r'|$) of a random sample x′ and y′ drawn from the population with zero correlation would be greater than or equal to the absolute value of the given sample ($|r|$) (https://docs.scipy.org/doc/scipy/reference/generated/scipy.stats.pearsonr.html). For this calculation, we considered the AV and orography matrix of each RCM member. Consequently, those members lacking orography information (Table 1) were excluded from the analysis.

Table 1 EURO-CORDEX RCM ensemble members and their corresponding driving GCMs used for this analysis

Institution/driving model	Member	Code	RCM	Variables
CCCma-CanESM2	r1i1p1	1	CLMcom-CCLM4-8-17	pr; tmin; tmax; orog
CCCma/CanESM2	r1i1p1	1	GERICS-REMO2015	pr; tmin; tmax; orog
CNRM-CERFACS/CNRM-CM5	r1i1p1	2	CLMcom-CCLM4-8-17	pr; tmin; tmax
CNRM-CERFACS/CNRM-CM5	r1i1p1	2	CLMcom-ETH	pr; tmin; tmax; orog
CNRM-CERFACS/CNRM-CM5	r1i1p1	2	CNRM-ALADIN63	pr; tmin; tmax; orog
CNRM-CERFACS/CNRM-CM5	r1i1p1	2	DMI-HIRHAM5	pr; tmin; tmax; orog
CNRM-CERFACS/CNRM-CM5	r1i1p1	2	GERICS-REMO2015	pr; tmin; tmax; orog
CNRM-CERFACS/CNRM-CM5	r1i1p1	2	IPSL-WRF381P	pr; tmin; tmax
CNRM-CERFACS/CNRM-CM5	r1i1p1	2	KNMI-RACMO22E	pr; tmin; tmax; orog
CNRM-CERFACS/CNRM-CM5	r1i1p1	2	MOHC-HadREM3-GA7-05	pr; tmin; tmax; orog
CNRM-CERFACS/CNRM-CM5	r1i1p1	2	RMIB-UGent-ALARO-0	pr
CNRM-CERFACS/CNRM-CM5	r1i1p1	2	SMHI-RCA4	pr; tmin; tmax; orog
ICHEC/EC-EARTH	r12i1p1	4	CLMcom-CCLM4-8-17	pr; tmin; tmax; orog
ICHEC/EC-EARTH	r12i1p1	4	CLMcom-ETH	pr; tmin; tmax
ICHEC/EC-EARTH	r12i1p1	4	DMI-HIRHAM5	pr; tmin; tmax; orog
ICHEC/EC-EARTH	r12i1p1	4	GERICS-REMO2015	pr; tmin; tmax; orog
ICHEC/EC-EARTH	r12i1p1	4	ICTP-RegCM4-6	pr; tmin; tmax; orog
ICHEC/EC-EARTH	r12i1p1	4	IPSL-WRF381P	tmin; tmax
ICHEC/EC-EARTH	r12i1p1	4	KNMI-RACMO22E	pr; tmin; tmax; orog
ICHEC/EC-EARTH	r12i1p1	4	MOHC-HadREM3-GA7-05	pr; tmin; tmax; orog
ICHEC/EC-EARTH	r12i1p1	4	SMHI-RCA4	pr; tmin; tmax; orog
ICHEC/EC-EARTH	r12i1p1	4	UHOH-WRF361H	pr; tmin; tmax
ICHEC/EC-EARTH	r1i1p1	3	CLMcom-ETH	pr; tmin; tmax
ICHEC/EC-EARTH	r1i1p1	3	DMI-HIRHAM5	pr; tmin; tmax; orog
ICHEC/EC-EARTH	r1i1p1	3	KNMI-RACMO22E	pr; tmin; tmax; orog
ICHEC/EC-EARTH	r1i1p1	3	SMHI-RCA4	pr; tmin; tmax; orog
IPSL/IPSL-CM5A-MR	r1i1p1	6	DMI-HIRHAM5	pr; tmin; tmax
IPSL/IPSL-CM5A-MR	r1i1p1	6	GERICS-REMO2015	pr; tmin; tmax; orog
IPSL/IPSL-CM5A-MR	r1i1p1	6	IPSL-WRF381P	pr; tmin; tmax
IPSL/IPSL-CM5A-MR	r1i1p1	6	KNMI-RACMO22E	pr; tmin; tmax; orog
IPSL/IPSL-CM5A-MR	r1i1p1	6	SMHI-RCA4	pr; tmin; tmax; orog
MIROC/MIROC5	r1i1p1	7	CLMcom-CCLM4-8-17	pr; tmin; tmax; orog
MIROC/MIROC5	r1i1p1	7	GERICS-REMO2015	pr; tmin; tmax; orog
MIROC/MIROC5	r1i1p1	7	UHOH-WRF361H	pr
MOHC/HadGEM2-ES	r1i1p1	5	CLMcom-CCLM4-8-17	pr; tmin; tmax; orog
MOHC/HadGEM2-ES	r1i1p1	5	CLMcom-ETH	pr; tmin; tmax
MOHC/HadGEM2-ES	r1i1p1	5	CNRM-ALADIN63	pr; tmin; tmax; orog
MOHC/HadGEM2-ES	r1i1p1	5	DMI-HIRHAM5	pr; tmin; tmax; orog
MOHC/HadGEM2-ES	r1i1p1	5	GERICS-REMO2015	pr; tmin; tmax; orog
MOHC/HadGEM2-ES	r1i1p1	5	ICTP-RegCM4-6	pr; tmin; tmax; orog
MOHC/HadGEM2-ES	r1i1p1	5	IPSL-WRF381P	pr; tmin; tmax
MOHC/HadGEM2-ES	r1i1p1	5	KNMI-RACMO22E	pr; tmin; tmax; orog
MOHC/HadGEM2-ES	r1i1p1	5	MOHC-HadREM3-GA7-05	pr; tmin; tmax; orog
MOHC/HadGEM2-ES	r1i1p1	5	SMHI-RCA4	pr; tmin; tmax; orog
MOHC/HadGEM2-ES	r1i1p1	5	UHOH-WRF361H	pr; tmin; tmax
MPI-M/MPI-ESM-LR	r1i1p1	8	CLMcom-CCLM4-8-17	pr; tmin; tmax; orog
MPI-M/MPI-ESM-LR	r1i1p1	8	CLMcom-ETH	pr; tmin; tmax
MPI-M/MPI-ESM-LR	r1i1p1	8	CNRM-ALADIN63	pr; tmin; tmax; orog
MPI-M/MPI-ESM-LR	r1i1p1	8	DMI-HIRHAM5	pr; tmin; tmax; orog
MPI-M/MPI-ESM-LR	r1i1p1	8	ICTP-RegCM4-6	pr; tmin; tmax; orog
MPI-M/MPI-ESM-LR	r1i1p1	8	IPSL-WRF381P	pr; tmin; tmax

Table 1 (continued)

Institution/driving model	Member	Code	RCM	Variables
MPI-M/MPI-ESM-LR	r1i1p1	8	KNMI-RACMO22E	pr; tmin; tmax; orog
MPI-M/MPI-ESM-LR	r1i1p1	8	MOHC-HadREM3-GA7-05	pr; tmin; tmax; orog
MPI-M/MPI-ESM-LR	r1i1p1	8	MPI-CSC-REMO2009	pr; tmin; tmax
MPI-M/MPI-ESM-LR	r1i1p1	8	SMHI-RCA4	pr; tmin; tmax; orog
MPI-M/MPI-ESM-LR	r1i1p1	8	UHOH-WRF361H	pr; tmin; tmax; orog
MPI-M/MPI-ESM-LR	r2i1p1	9	CLMcom-ETH	pr; tmin; tmax
MPI-M/MPI-ESM-LR	r2i1p1	9	MPI-CSC-REMO2009	pr; tmin; tmax; orog
MPI-M/MPI-ESM-LR	r2i1p1	9	SMHI-RCA4	pr; tmin; tmax; orog
MPI-M/MPI-ESM-LR	r3i1p1	10	CLMcom-ETH	pr; tmin; tmax
MPI-M/MPI-ESM-LR	r3i1p1	10	GERICS-REMO2015	pr; tmin; tmax; orog
MPI-M/MPI-ESM-LR	r3i1p1	10	SMHI-RCA4	tmin; tmax; orog
NCC/NorESM1-M	r1i1p1	11	CLMcom-ETH	pr; tmin; tmax
NCC/NorESM1-M	r1i1p1	11	CNRM-ALADIN63	pr; tmin; tmax; orog
NCC/NorESM1-M	r1i1p1	11	DMI-HIRHAM5	pr; tmin; tmax; orog
NCC/NorESM1-M	r1i1p1	11	GERICS-REMO2015	pr; tmin; tmax; orog
NCC/NorESM1-M	r1i1p1	11	ICTP-RegCM4-6	pr; tmin; tmax; orog
NCC/NorESM1-M	r1i1p1	11	IPSL-WRF381P	pr; tmin; tmax
NCC/NorESM1-M	r1i1p1	11	KNMI-RACMO22E	pr; tmin; tmax; orog
NCC/NorESM1-M	r1i1p1	11	MOHC-HadREM3-GA7-05	pr; tmin; tmax; orog
NCC/NorESM1-M	r1i1p1	11	SMHI-RCA4	pr; tmin; tmax; orog

The column "Variables" includes the variables that have been taken into account for each of the members

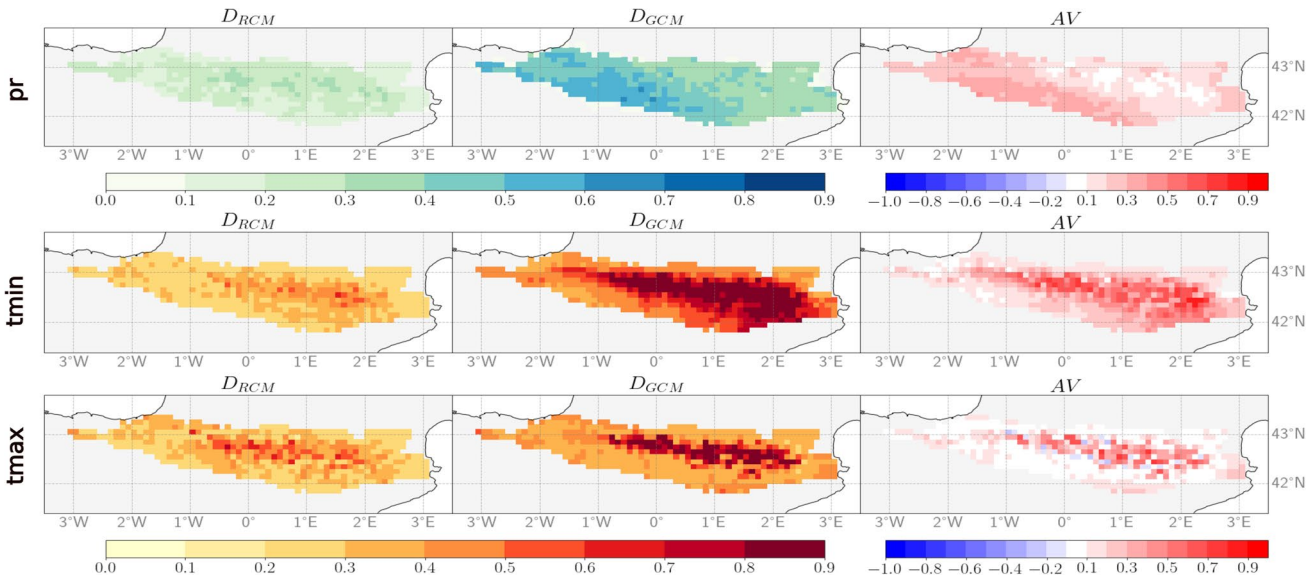

Fig. 2 Relative probability difference (D_M in (1)) of the RCM (left column) and the GCM (middle column) and the added value (AV in (2); right column) of the ensemble means at 0.11° resolution, for precipitation (top row), minimum temperature (middle row) and maximum temperature (bottom row) using CLIMPY as reference over the period 1981–2015

3 Results

3.1 Added Value for the entire PDFs

Figure 2 illustrates the relative probability difference (D_M; (1)) of the RCM and GCM ensemble means, and the resulting added value index (AV in (1)) for the three analyzed variables. Regarding precipitation, the D_{RCM} exhibits values between 0.2 to 0.4 uniformly distributed across the region. In contrast, D_{GCM} displays a latitudinal gradient with higher values on the southern slope of the mountain range (~ 0.7) and lower values on the northern part (~ 0.3). Consequently, the resulting AV index indicates better performance of the RCMs with notable improvement in the central zone of the southern slope where the GCM ensemble-mean performs poorly.

In terms of minimum temperature, homogeneous values of the D_{RCM} ensemble mean across almost the entire mountain range were observed. This contrasts with the values of D_{GCM}, which exceed 0.8 in the highest regions as well as on the eastern area of the southern slope. Consequently, a significantly high AV is observed in these areas, where the GCM ensemble mean exhibits inadequate performance. The results for maximum temperature demonstrate a similar pattern, but with some distinctions. Although the D_{GCM} is also higher in high-elevation regions, it is more localized compared to the case of minimum temperature, suggesting that, overall, the GCM ensemble mean represents maximum temperatures more accurately than minimum temperatures. The AV for maximum temperature reaches its highest values in the central region, surrounded by values close to 0.

Figure 3 exhibits a parallel structure to Fig. 2, albeit with data upscaled to the native resolution of the GCM (1.00°). Remarkably, the findings for both D and AV remain consistent across the two resolutions. However, due to the coarse spatial resolution and the relatively small coverage area of the Pyrenees, our analysis is confined to a grid of only five cells. Despite this limitation, the obtained information aligns with the spatial distribution depicted in Fig. 2. In the case of precipitation, the AV at 1.00° resolution shows maximal values in the western sector of the mountain range. This phenomenon is related with a poor GCM performance, as evidenced by high D_{GCM} values. Conversely, for tmin, the highest AV is observed in the central–eastern area of the Pyrenees, corresponding to the region of highest elevation (Fig. 1). Finally, for tmax, AV values are notably lower, with instances of negative values occurring in the lower altitude zones of the mountain range.

The conclusions derived from analyzing the ensemble mean overlook the signals provided by each individual member. Figures A1–A3 present the AV a 0.11° for the individual members in a matrix format, where the rows represent the

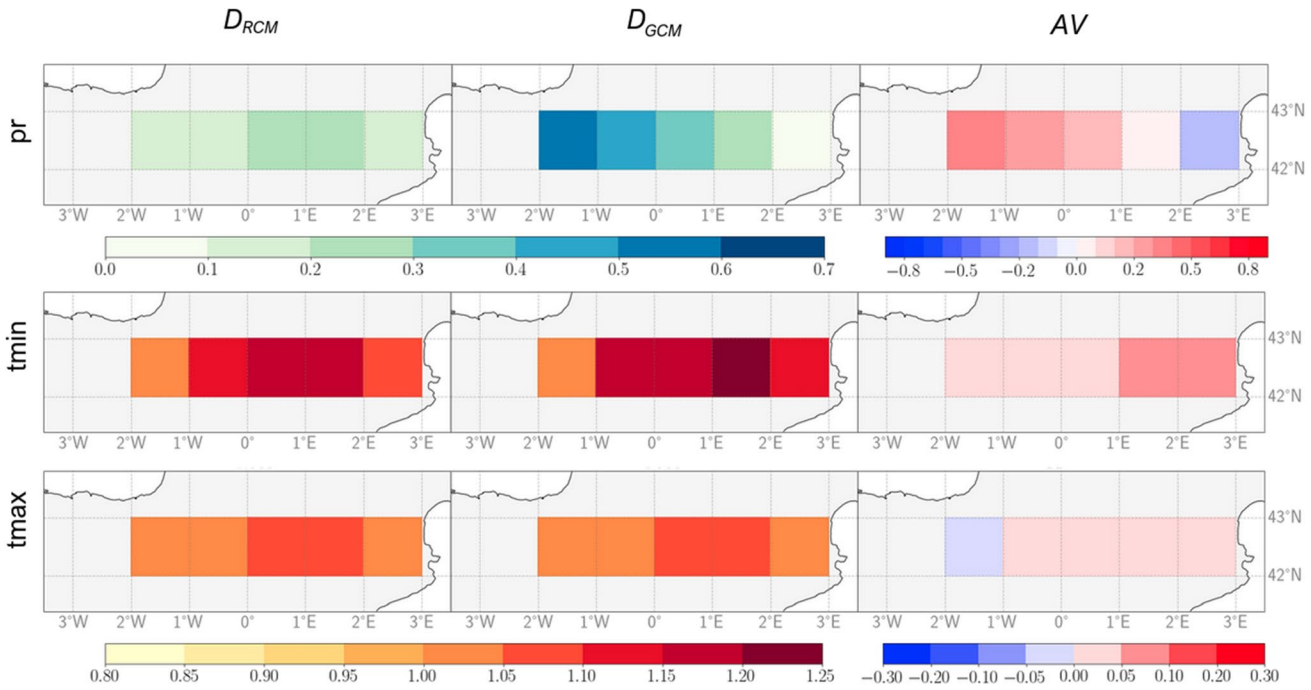

Fig. 3 Relative probability difference (D_M in (1)) of the RCM (left column) and the GCM (middle column) and the added value (AV in (2); right column) of the ensemble means at 1.00° resolution, for precipitation (top row), minimum temperature (middle row) and maximum temperature (bottom row) using CLIMPY as reference over the period 1981–2015

GCM driver and the columns represent the RCM. Similarly, Figs. A4–A6 present this same information but for the calculation performed at a resolution of 1.00°. The results are consistent for both fine and coarse resolution. Concerning precipitation, the AV demonstrates a stronger dependence on the GCM rather than the RCM, aligning with the findings of Ciarlo et al. (2021) and Di Luca et al. (2016). The groups of models driven by CanESM (Code 1), CNRM (Code 2), and NCC (Code 11) exhibit the highest AV, while the models driven by MPI (Codes 8 and 9) yield lower AVs, occasionally even showing negative values, meaning that MPI GCMs (Codes 8 and 9) have an excellent performance over the Pyrenees. The spatial distribution of the AV in all members follows a consistent pattern observed in Fig. 2, with lower AV values in higher-elevation areas of the mountain range. Regarding temperatures, the predominance of the GCMs in the AV result is less evident. However, for both minimum and maximum temperatures, the models driven by CNRM (Code 2) show lower AVs at both resolutions, which in the case of coarse resolution is also evident for the EC-EARTH GCM (Codes 3 and 4). In the case of minimum temperature, the contribution of the RCMs to the AV signal is especially noticeable, particularly with the RCM models RCA4 and RACMO22E, which have a negative influence on representing the variable's mean. Conversely, in the case of maximum temperature, the RCM model REMO2019 positively shapes the AV signal, particularly at 0.11° resolution.

3.2 Added value for percentile intervals

It is particularly important to focus on specific intervals of the PDF to gain insights into how the models perform in the tails of the distribution, which are associated with unusual events. Figure 4 provides a visual representation of the AV index at 0.11° resolution as a function of percentile intervals. Two approaches are considered: one with

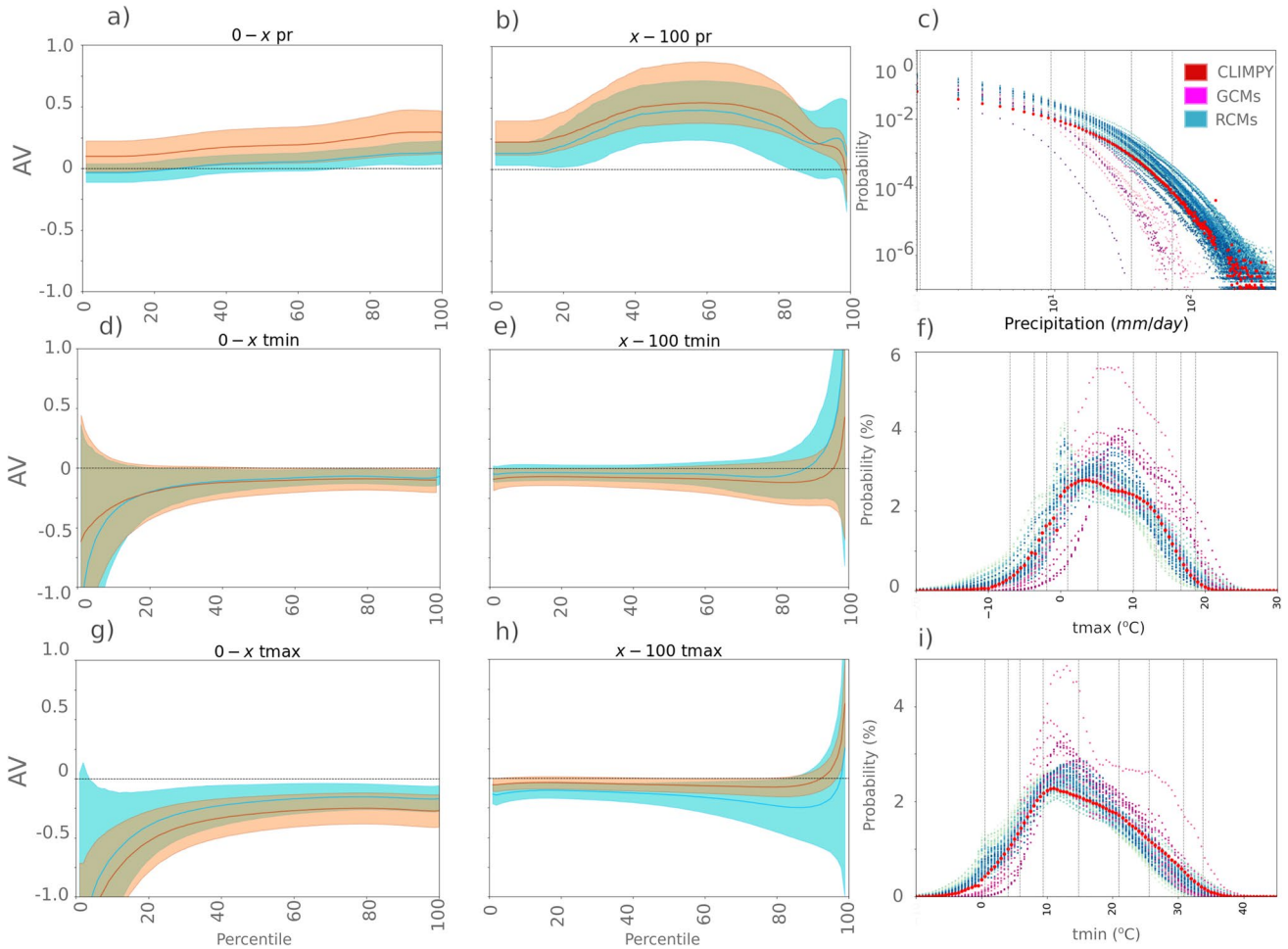

Fig. 4 Evolution of the mean and variability of the members (orange) and the ensemble and its spatial variability (blue) of the added value index (AV in (2)) as a function of the percentile intervals on the first and second columns for the variables "pr" (**a**, **b**), "tmin" (**d**, **e**) and "tmax" (**g**, **h**). The third column shows the PDFs of the observations (red), RCM members (blue), and GCM members (pink) and the CLIMPY percentiles for "pr" (**c**), "tmin" (**f**) and "tmax" (**i**)

0 percentile as the lower limit of the interval (0–x) and another with 100 percentile as the upper limit (x–100). The percentiles are varied from 1 to 100 in the first case and from 99 to 0 in the second case. Figure 4 displays two curves: the orange line represents the average AV index of all members as a function of percentile, while the orange shading represents inter-member variability; the blue curve, on the other hand, illustrates the evolution of the AV index of the ensemble mean shown in Fig. 2 as a function of percentile. The blue line represents the spatial average for the entire region, while the blue shading represents spatial variability.

In terms of precipitation, the AV index gradually increases for the 0–x case, indicating a lower AV at the left end of the distribution, which corresponds to minimum precipitation values (< 1 mm/day), including dry events. This observation is corroborated when considering the x–100 case, where overall, the AV values are higher compared to the 0–x case. Furthermore, as the 100th percentile was approached, the AV index increases. These results suggest that RCMs struggle to accurately represent events located in the left extreme of the precipitations PDF. In the 90–100 interval, a minimum in the AV index is observed, followed by a slight increase. To gain a better understanding of this trend, Fig. 4c includes the probability density functions (PDFs) of all members and observations. The PDFs demonstrate that all members (RCMs and GCMs) overestimate low-intensity events, a characteristic linked to the well-known drizzle phenomenon: both RCMs and GCMs exhibit a pattern of background light rain events persisting throughout the year, yet they inadequately capture episodes of zero rainfall (Coppola et al. 2021; Kämäräinen et al. 2018; van Meijgaard and Crewell 2005). From 10 mm/day values and onwards, which corresponds to the 90th percentile, the GCMs start to underestimate precipitation, while the RCMs remarkably reproduce the PDF of the observations. The inflection point occurs around the 90th percentile, where the curve of the observations intersects with the curves of the GCMs. This intersection explains the existence of the minimum in Fig. 4b at the 90th percentile.

Both maximum and minimum temperatures exhibit similar behavior. In the 0–x interval, the AV index reaches very low values, stabilizing around −0.2 when x is below the 20th percentile in both cases. The orange shaded areas represent the variability among members, which is considerable in intervals with $x < 20$. This indicates that the members considered present diverse AV values, ranging from positive to negative values. The spatial variability (shaded in blue) follows the same pattern. In the 0–x intervals where $x < 20$, the shaded area exhibits significant amplitude. In summary, this suggests that the AV index will vary considerably depending on the spatial location and RCM member in the lower tails of the temperature distribution.

Conversely, in the x–100 interval, the AV index increases in the right tail of the distribution when the 100th percentile is included. These results indicate that dynamical downscaling provides added value in the right tail of the maximum and minimum temperature distribution, corresponding to the warm events of both temperatures. However, it diminishes the quality of the simulation in the left tail of the distribution, which represents the minimum temperature values, associated with cold events.

In terms of the temperature PDFs (Fig. 4f, i), it is worth noting that they exhibit a similar shape to the observations, with improvements observed in the fit for the RCMs. The GCMs consistently overestimate the maxima and underestimate the minima of both temperatures, although the dynamic downscaling corrects the overestimation for the maxima. In the lower tail of the distribution, however, the RCMs overestimate the number of minimum events for both temperatures, resulting in negative AV values (Fig. 4d, g).

Figures 5, 6 and 7 provide insights into the spatial distribution of the AV of the ensemble mean for specific intervals, and these results align with the trends observed in Fig. 4. In the case of precipitation (Fig. 5), there is a gradual increase in AV for the 0–x interval, as depicted in Fig. 4a. Furthermore, the x–100 interval exhibits higher AV values compared to the 0–x interval, confirming the observations in Fig. 4b and indicating a very low AV near the zero percentile. When considering the spatial distribution of AVs, lower values are observed in the higher regions of the mountain range. As x increases, these regions expand and decrease in value, occasionally reaching negative values in certain areas. Consequently, a minimum AV occurs at the 90th percentile, which corresponds to the intersection between the PDFs of the GCMs and RCMs (Fig. 4c).

The detection of low AV at high elevations may be linked to deficiencies in precipitation observations within these areas. In high-mountain regions, such as the Pyrenees, lower station density is prevalent due to their remote locations (Isotta et al. 2014). Coupled with the lack of calibration for under-catch gauges, which can lead to underestimation of precipitation, particularly in windy and snowy conditions, the observations may not accurately represent the precipitation patterns in higher elevation regions (Adam and Lettenmaier 2003; Torma et al. 2015). These observation biases have the potential to influence the AV index, thereby limiting the reliability of the results at high altitudes.

Figure 5 also reveals an interesting feature of the AV index within the 99.9–100 interval, where a decrease in AV across the entire region is observed. This phenomenon occurs due to the small number of events within this interval, each event being classified into bins based on its magnitude. Although dynamical downscaling improves the representation of the upper tail of the distribution, it struggles to accurately predict the magnitude of these rare events,

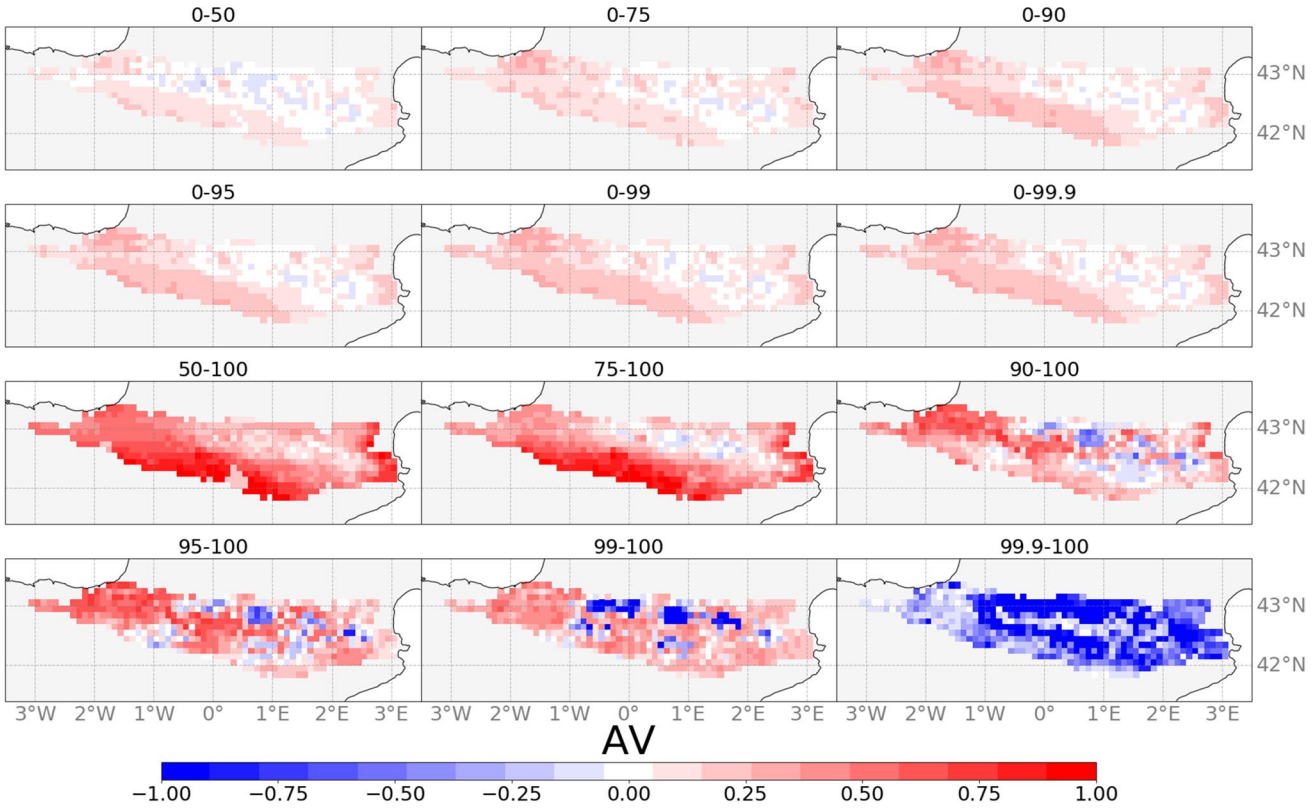

Fig. 5 Added value index (AV in (2)) for RCM ensemble mean at different percentile intervals at 0.11° × 0.11° for precipitation variable using CLIMPY as reference over the period 1981–2015

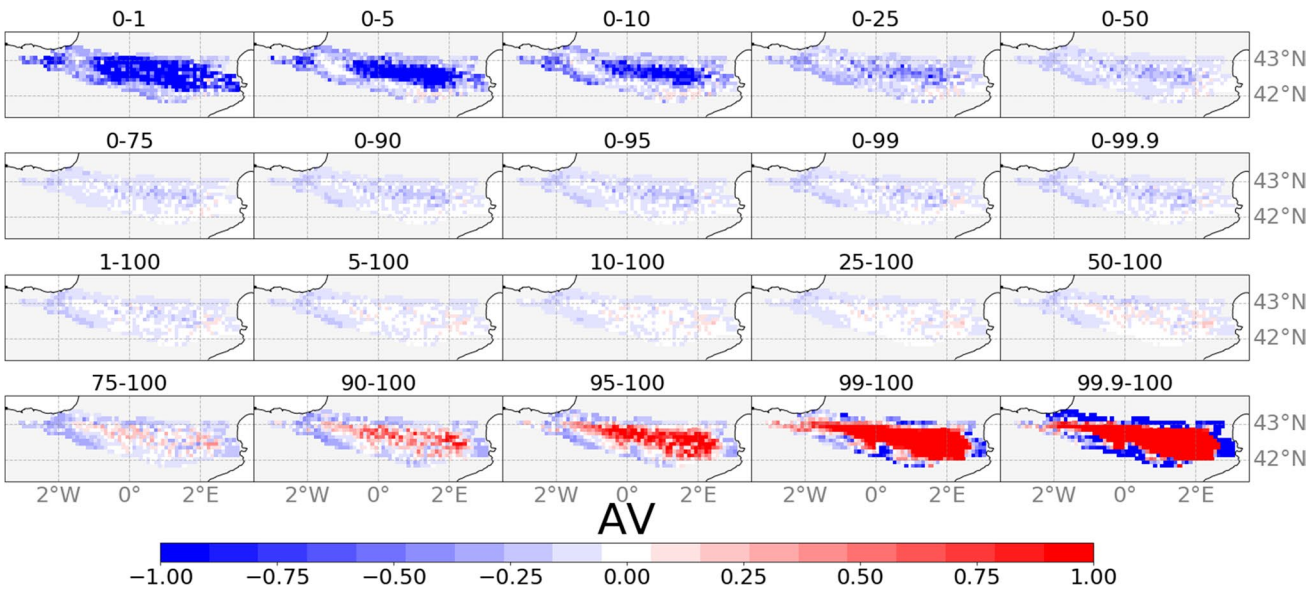

Fig. 6 Added value index (AV in (2)) for RCM ensemble mean at different percentile intervals at 0.11° × 0.11° for minimum temperature variable using CLIMPY as reference over the period 1981–2015

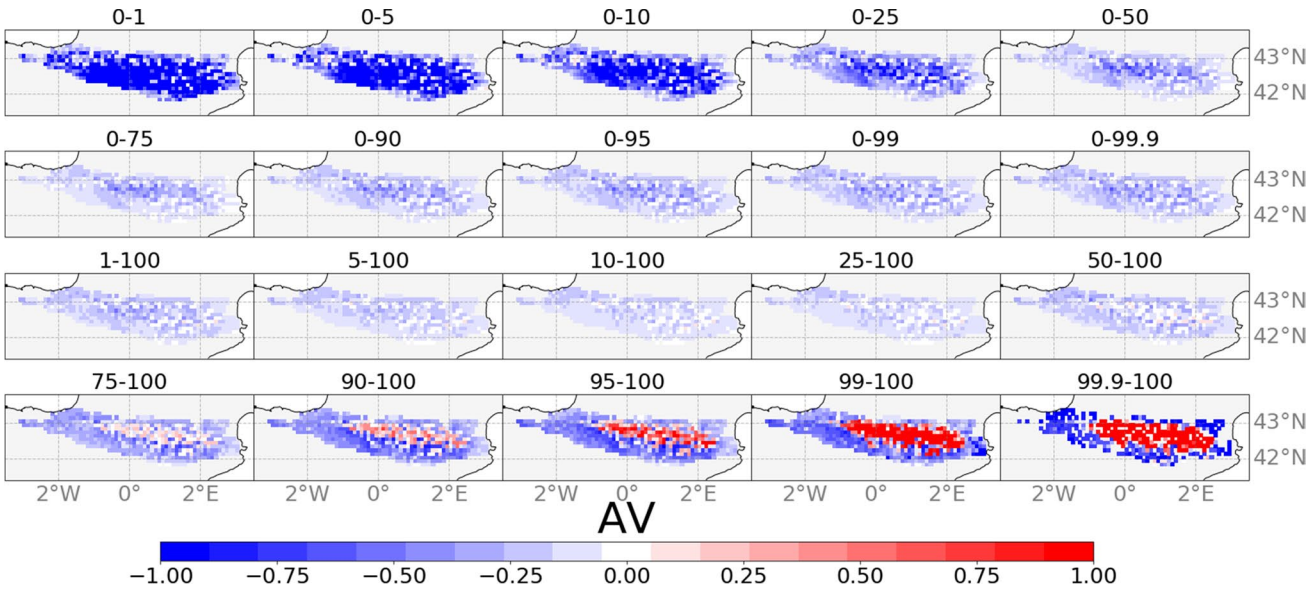

Fig. 7 Added value index (AV in (2)) for RCM ensemble mean at different percentile intervals at 0.11° × 0.11° for maximum temperature variable using CLIMPY as reference over the period 1981–2015

causing them to be placed in different bins compared to the observations. Consequently, when comparing the frequency of events in each bin, the AV decreases. Given the minimal number of events, this does not significantly impact the overall AV index of the PDF.

The results for minimum and maximum temperatures in Figs. 6 and 7 also exhibit consistency with Fig. 4b, c. The right tail of the distribution, which corresponds to minimum events, demonstrates a very low AV. The AV remains consistently low throughout the evolution of the interval, but when reaching the 90–100 range, it experiences an exponential increase, yielding considerably high values in the central region of the mountain range. This positive AV signal aligns with the mean spatial distribution depicted in Fig. 2. In essence, the presence of positive mean AV values for both maximum and minimum temperatures is influenced by the AV of the upper end tail of the distribution.

The most notable distinction between the evolution of the AVs for minimum and maximum temperatures lies in their spatial extent. In the case of minimum temperature, the positive AVs cover a larger area and reach higher values. Conversely, the positive AVs associated with maximum temperature remain more localized within the higher elevations of the mountain range, surrounded by negative AVs.

3.3 Added value evolution with orography

Considering the apparent correlation between the AV index and elevation, Fig. 8 provides insight into the correlations between the AV mean and elevation for the Pyrenean region, allowing for a more comprehensive exploration of their spatial relationships. The scatter plot of precipitation (Fig. 8.a) shows a negative relationship between ensemble mean AV and elevation, although the AV remains positive for the entire elevation range, consistent with Fig. 2. Likewise, precipitation demonstrates a widespread negative correlation across nearly all members (Fig. 8b), implying that as elevation increases, the AV index tends to decrease. This findings aligns with the outcomes obtained in Sects. 3.1 and 3.2, suggesting that while remains positive across the entire region there is a limitation of AV at higher elevations potentially related to constraints within the observational dataset at these altitudes. The set of models driven by CanESM2 (Code 1) exhibits notable positive correlation values, which can potentially be attributed to the widespread misrepresentation of precipitation by this GCM that is significantly improved through the dynamical downscaling process across the entire region.

Conversely, the relationship between AV and elevation for both temperatures demonstrate positive values, implying higher AV in the elevated regions. However, there are some distinctions in the scatter plots of tmax and tmin (Fig. 8a): while the AV for the tmax ensemble mean does not show a clear increase with elevation from 0 to 1500 m, beyond 1500 m, there is a significant rise. In the case of tmin the positive relationship of AV and elevation is constant for the whole elevation range. Similarly, the correlation coefficients of the individual members are also generally positive (Fig. 8b). This observations align with the findings illustrated in Figs. 6 and 7. However, it is worth noting that there are some exceptions where negative correlation coefficients are observed. Specifically, in the model group driven

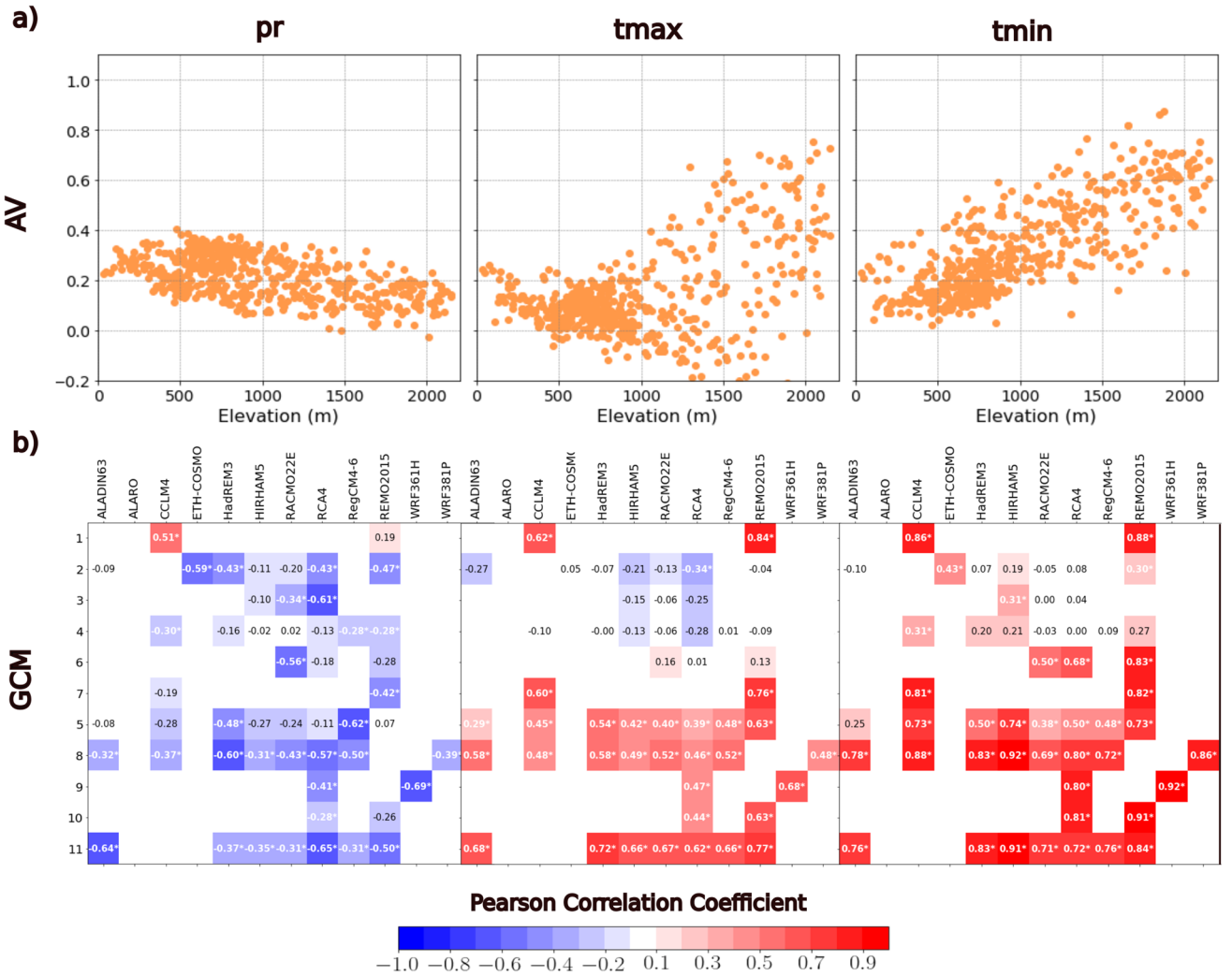

Fig. 8 **a** AV vs. elevation scatter plots for the ensemble mean for the variables precipitation, maximum temperature and minimum temperature. **b** Correlation coefficients between AV and elevation for all members of the variables precipitation, maximum temperature and minimum temperature. The matrix is formed by the RCMs (x axis) and the GCMs (y axis) expressed as the codes defined in Table 1. Asterisk (*) indicates a statistically significant correlation at 95% from t-Student test.e and minimum temperature. Asterisk (*) indicates a statistically significant correlation at 95% from t-Student test

by CNRM (Code 2) and by EC-EARTH (Codes 3 and 4), these negative correlations can be attributed to the excellent performance of the GCM, which limits the RCM's ability to improve the representation of the variable AV in those cases.

Figure 9 shows the evolution of the correlation coefficients between AV and elevation as a function of the percentile intervals, following a similar approach of Fig. 4. The evolution of the AV of precipitation remains constant. However, the temperature results lead us to the conclusion that the positive correlations observed for the entire PDF (Fig. 8) are influenced by the upper tail of the distribution. This indicates that dynamic downscaling enhances the representation of warm events in the higher regions. However, negative correlation values were noted in the lower end of the temperature distributions. This, combined with the low AV values of the temperatures in the lower tails (Fig. 4d, g, 6, 7), suggests that the inadequacy of the lowest tails of representation of the temperatures by the RCMs is primarily located in the high altitude regions.

4 Discussion

There is a clear positive added value of using high-resolution RCMs derived from a dynamically downscaling of low-resolution GCMs, rather than using the latter, particularly in relation to precipitation at both resolutions: at 0.11° (Fig. 2) and at 1.00° (Fig. 3). This finding aligns with previous studies analyzing precipitation at European scale, including topographically complex regions such as the Alpine Range and

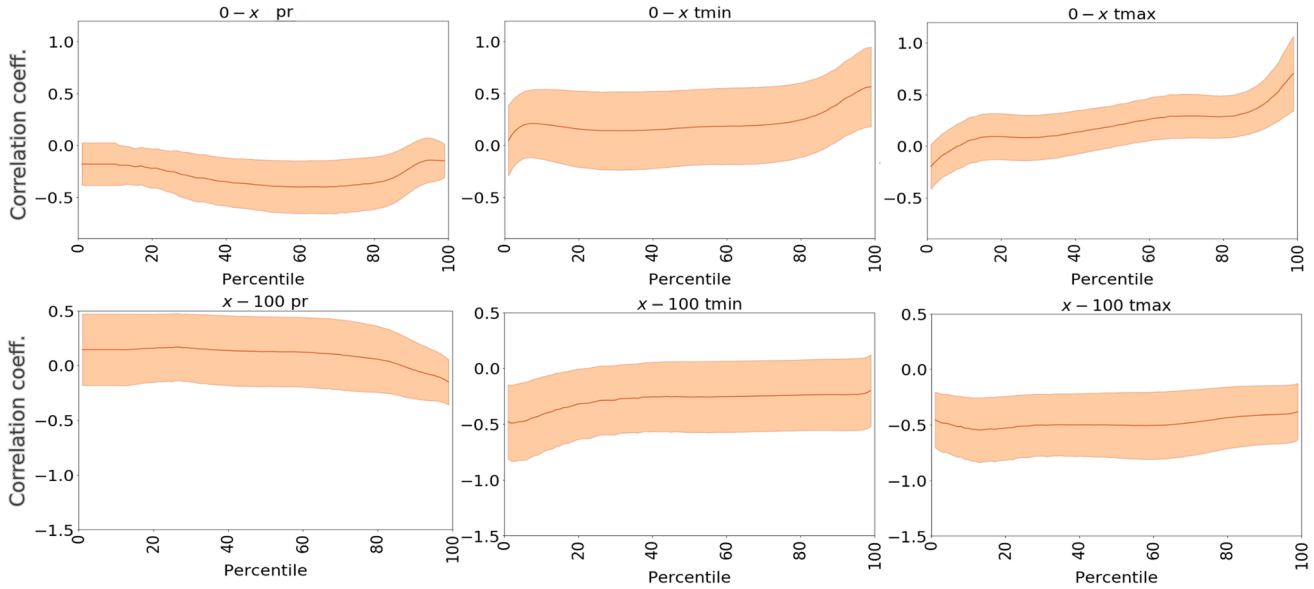

Fig. 9 The variability of the correlation coefficients between AV index (AV in (2)) compared to CLIMPY, and elevation at different percentile intervals for "pr", "tmin" and "tmax". Each point x describes the correlation coefficient of the percentile interval "0–x" (up), and "x–100" (down). The shaded area shows the standard deviation of the members

the Iberian Peninsula, among others (Careto et al. 2022b; Terzago et al. 2017). The improvement of simulating precipitation in the RCMs can be attributed to a better representation of topographically induced local circulation due to an increase in the spatial resolution (Careto et al. 2022b). Also, Prein et al. (2016) suggested that this positive AV stems from a more accurate depiction of precipitation in areas influenced by prevailing westerly winds, particularly evident during winter months when synoptic-scale flow plays a dominant role in the European sector. This is consistent with our results showing an increase in the AV index, particularly in the western part of the Pyrenees where westerly disturbances coming from the Atlantic Ocean contribute the most to winter precipitation.

Similarly, in the case of maximum and minimum temperatures, a positive AV is identified when using RCMs, particularly in higher elevation areas of the Pyrenees in both resolutions (Figs. 2 and 3). Specifically, a more extensive positive AV is observed for minimum temperatures compared to the maximum temperatures which is consistent with the conclusions drawn by Cardoso and Soares (2022), who found larger positive AVs for the minimum temperature than for the maximum temperature in Europe. The high AV values for minimum temperatures can be attributed to the GCMs' potential misrepresentation of orographically induced minimum temperatures, which are automatically rectified by considering topographic features more accurately through resolution refinement (Perkins et al. 2007). In fact, Di and Ramo (2013) established that the potential added value of 2-m temperature provided by RCMs in the North American region, particularly in areas with complex topography, could be directly attributed to more than 65% of orographically induced simple interactions. Specifically, this pertains to the general correlation between temperature and terrain elevation. Thus, a more detailed representation of elevation gradients would significantly enhance the temperature portrayal of GCMs, even in the absence of fine-scale atmospheric processes. Consequently, it remains to be determined the extent to which the achieved AV might be mitigated by considering the simple relationships between high-resolution surface forcing and the low-resolution maximum and minimum temperatures. Additionally, Cardoso and Soares (2022) suggest that positive AV values for maximum temperatures over the Iberian Peninsula are associated with improved representations of precipitation and snow, mainly regarding the better representation of snow free surfaces.

It is important to note that significant variations exist in the signals of individual members (Figs. A1–A6) at both resolutions, indicating substantial dependence of the AV on the driving GCM. This behavior underscores the notion that the quality of the GCM driver may limit the RCM's ability to enhance the representation of the variable. In the case of precipitation, the excellent performance of the MPI-ESM-LR model (Codes 8 and 9; Brands et al. 2013) leads to lower AV values. However, for the EC-EARTH GCM (Codes 3 and 4), characterized by good precipitation representations ($D_{GCM} = 0.32$ and 0.29 respectively for 0.11° resolution), the downscaling continues to yield significant AV values. This observation suggests the presence of other influential factors shaping the relationships between the AV and the models.

One such factor may involve the accurate or deficient positioning of storm tracks by the GCMs. Dynamic downscaling holds promise for enhancing precipitation characterization, provided the GCM accurately identifies the positioning of storm tracks. However, if the GCM fails to do so, the potential AV of the RCM may be limited. Indeed, Zappa et al. (2013) highlight the importance of correct storm track positioning for the EC-EARTH GCM (Codes 3 and 4). Conversely, the HadGEM GCM (Code 5) exhibits similar D_{GCM} values (0.27) to EC-EARTH, yet dynamic downscaling does not lead to an improved variable characterization, resulting in a lower AV. This discrepancy could be attributed to the model's poor positioning of storm tracks during the summer months at the longitudes of the study area (Zappa et al. 2013). Likewise, for both minimum and maximum temperature, GCMs with better performance, such as CNRM-CM5 (Code 2; McSweeney et al. (2015)), restrict the AV achieved through dynamic downscaling using RCMs. In other words, a low D_{GCM}, indicating a better variable representation by the GCM, constrains the RCMs' capacity to improve upon that representation, resulting in diminished AVs. Despite the nuanced character of the improvements brought about by downscaling in this context, they remain pertinent in certain instances. For instance for the 0.11° resolution, in the CNRM+CLMcom-ETH model, low and comparable D_{GCM} values are observed for both tmax and tmin, standing at 0.31 and 0.33, respectively. However, while the AV of downscaling for tmax is nearly zero (−0.007), for tmin it stands at 0.12, signifying a noteworthy enhancement in variable representation. Similarly, the EC-EARTH driver exhibits Dgcm values around 0.41 for both temperature variables and the RCM RCA4 manages to improve tmax representation by 0.03, while the AV for tmin approaches zero.

The employed methodology allows for a more in-depth examination of AV through different intervals of the probability density function (PDF). It is observed that all GCMs consistently underestimate high rainfall events, while exhibiting an overrepresentation of light rainfall events (Fig. 4c), as also been highlighted by Perkins et al. (2007). RCMs succeed in significantly improving the representation of events above the 90th percentile, as reflected in the AV's evolution relative to the percentile, particularly evident in the x–100 case (Fig. 4b). However, for precipitation rates below 10 mm/day, RCMs record higher precipitation values than observations, resulting in an intersection between the PDF of observations and the PDFs of RCMs. This intersection is also evident in Fig. 4b, manifesting a minimum in the AV (Ciarlo et al. 2021). Consequently, RCMs face challenges in representing light rainfall events and dry events (Boberg et al. 2009, 2010; Soares and Cardoso 2018; Careto et al. 2022b). It is important to acknowledge that while these limitations in reproducing minimum precipitation events exist, they are unlikely to significantly influence the characterization of total precipitation. This is because such events typically contribute minimally to the overall precipitation amount (Dai 2001).

At the spatial level (Fig. 5), the lowest AV values within percentile intervals (0–50, 0–75, 0–90) are concentrated in the easternmost extremity of the mountain range, characterized by a Mediterranean climate (Lemus-Canovas et al. 2019), where water recycling through soil moisture-atmosphere feedback plays a critical role (RiosEntenza et al. 2014; Careto et al. 2022b), due to the importance of the contribution of evapotranspiration in the precipitation regime, especially in the summer months, which could lead to an overrepresentation of light precipitation events.

Further exploration of the contributions of PDF intervals to temperature AV reveals that while the AV remains close to zero around the mean values of the PDF, it is the tails ends of the temperature PDFs that shape the signal. GCMs tend to overestimate higher percentile events while underestimating the lower tail events (Fig. 4f, i), in line with the findings of Perkins et al. (2007). Dynamical downscaling significantly improves the representation of upper tail extremes in both maximum and minimum temperatures, primarily over the central region of the Pyrenees characterized by higher elevations. Moreover, greater benefits are observed for minimum temperatures compared to maximum temperatures (Cardoso and Soares 2022). Conversely, there is a general decline in the representation of lower tails for both temperatures, indicating that dynamical downscaling has a negative effect on simulating cold extremes. Additionally, difficulties arise in representing accurately near-freezing temperatures (Fig. 4f, i), leading to an overestimation of maximum and minimum temperatures close to 0°C, as also noted by Careto et al. (2022a). These deficiencies in RCMs are associated with problems in simulating snow dynamics and its interactions, influencing snow-albedo feedback and surface flux partitioning. Terzago et al. (2017) reported thicker snowpack over the alpine ridge and shallower snowpack in lower elevation regions simulated by RCMs compared to observational datasets. Such biases in snowpack representation likely contribute to biases in simulated snow-albedo feedback and surface temperatures (Minder et al. 2016). These biases in extreme minimum temperatures manifest as negative AV values at the left extreme of the PDF for both temperatures, spreading across the entire Pyrenees area. An additional significant aspect of the added value regarding maximum and minimum temperatures is the presence of inter-member variability within the extreme tails of the distribution. This variability is closely linked to the GCMs' ability to simulate temperature patterns.

The findings additionally reveal significant correlations between AV values and orography in the Pyrenees region, emphasizing the significance of elevation when assessing the performance of climate simulations (Reder et al. 2020).

The negative correlation values point to a negative AV in high-altitude regions specially in high precipitation rates, potentially indicating the limited quality of observations at these points (Torma et al. 2015). Concerning temperatures, there exists a positive correlation at the right tail of the distribution, indicating that high AV values are concentrated in high-elevation regions in warm events. Conversely, a negative correlation in the left tail suggests that, for cold events, higher-altitude regions yield lower AV values.

5 Summary and conclusions

This study presents a comprehensive assessment of the added value provided by Regional Climate Models (RCMs) compared to Global Climate Models (GCMs) in the high mountain region of the Pyrenees for the variables precipitation, minimum temperature, and maximum temperature. To conduct this analysis, the CLIMPY observational database as a reference was employed. The assessment delves into both the spatial distribution of added value as well as the contribution of Probability Distribution Function (PDF) intervals of the analyzed variables to the overall added value.

The results obtained highlight a significant enhancement achieved through dynamical downscaling in accurately reproducing mean precipitation across the central and southwestern parts of the mountain range. Notably, these regions are influenced by westerly disturbances that play a key role in shaping the precipitation regime. The mean maximum and minimum temperatures also exhibit positive added values, particularly evident in the higher elevations of the Pyrenees and are potentially related to the spatial resolution refinement.

Examining the contributions of individual model members to the added value reveals a significant dependence on the quality of the GCM simulation. This dependency implies that the GCMs limits the RCMs capacity to enhance the representation of these variables effectively.

Analyzing the precipitation through PDF intervals uncovers that dynamical downscaling enhances precipitation events exceeding the 90th percentile, while hampers to adequately represent lower precipitation rates, notably in the eastern region where a Mediterranean climate prevails. The overestimation of low precipitation rates likely stems from an inadequate representation of water recycling through moisture–atmosphere feedback by RCM models. Negative added value values are registered in the higher Pyrenean regions, potentially attributed to observational data deficiencies.

Regarding the temperature percentile intervals, the impact of downscaling becomes particularly apparent at the extremes. These extreme events also exhibit amplified spatial and inter-member variability. RCMs showcase an improved ability to capture warm events in the highest regions compared to GCMs. Conversely, dynamical downscaling's effectiveness in representing cold extremes is compromised, especially in the elevated areas where snow dynamics wield more influence.

These findings underscore the significant contributions of RCMs in accurately characterizing precipitation, minimum temperature, and maximum temperature variables. Nevertheless, it remains imperative to recognize their limitations, thereby facilitating the responsible utilization of RCM data for both historical periods. In addition, this information obtained from a historical period analysis is valuable when applying future projections of climate models. Liang et al. (2008) claim that the main biases present in the historical simulation of both RCMs and GCMs are systematically propagated into the projected future climate at regional scales, suggesting that the strengths and weaknesses of RCMs pointed out by this study will also be reproduced for future scenarios. Therefore, being aware of these advantages/limitations is essential for a more informed application of such data in the development and implementation of adaptation plans and risk management strategies for the future. Notably, these limitations manifest themselves in the sparse portrayal of dry and cold events by RCMs. The former could be linked to the misinterpretation of evapotranspiration's impact on precipitation patterns in Mediterranean regions within the Pyrenees. The latter could be primarily attributed to the models' deficiency in effectively simulating snow dynamics. This challenge assumes particular significance in the elevated regions of the Pyrenees, where snow dynamics have a substantial influence. While the results obtained in this analysis point towards these hypotheses, a more specific seasonal analysis for precipitation variable would shed more light on the potential causes.

Supplementary Information The online version contains supplementary material available at https://doi.org/10.1007/s00382-024-07318-8.

Acknowledgements This research was supported by the Spanish Government through Ref. MDM-415 2017-0714 and Ref. CEX2021-001201-M funded by MCINI/AEI/10.13039/501100011033 and through the AEI-funded MicroFAME project (Ref. PID2022-140975NB-I00). Open Access funding provided by the University of Basque Country (UPV/EHU).

Funding Open Access funding provided thanks to the CRUE-CSIC agreement with Springer Nature. The authors have not disclosed any funding.

Data availability The simulated variables for precipitation, maximum temperature and minimum temperature were taken from CMIP5 and CORDEX public projects. The observational data for the three variables is available at: https://doi.org/10.5281/zenodo.3611126.

Declarations

Conflict of interest The authors declare no conflict of interest.

References

Adam JC, Lettenmaier DP (2003) Adjustment of global gridded precipitation for systematic bias. J Geophys Res: Atmos 108(9):1–15. https://doi.org/10.1029/2002jd002499

Amblar-Francés MP, Ramos-Calzado P, Sanchis-Lladó J et al (2020) High resolution climate change projections for the Pyrenees region. Adv Sci Res 17:191–208. https://doi.org/10.5194/asr-17-191-2020

Boberg F, Berg P, Thejll P et al (2009) Improved confidence in climate change projections of precipitation evaluated using daily statistics from the PRUDENCE ensemble. Clim Dyn 32(7–8):1097–1106. https://doi.org/10.1007/s00382-008-0446-y

Boberg F, Berg P, Thejll P et al (2010) Improved confidence in climate change projections of precipitation further evaluated using daily statistics from ENSEMBLES models. Clim Dyn 35(7):1509–1520. https://doi.org/10.1007/s00382-009-0683-8

Brands S, Herrera S, Fernández J et al (2013) How well do CMIP5 Earth System Models simulate present climate conditions in Europe and Africa?: a performance comparison for the downscaling community. Clim Dyn 41(3–4):803–817. https://doi.org/10.1007/s00382-013-1742-8

Cardoso RM, Soares PM (2022) Is there added value in the EURO-CORDEX hindcast temperature simulations? Assessing the added value using climate distributions in Europe. Int J Climatol 42(7):4024–4039. https://doi.org/10.1002/joc.7472

Careto JAM, Soares PMM, Cardoso RM et al (2022a) Added value of EURO-CORDEX high-resolution downscaling over the Iberian Peninsula revisited—part 2: max and min temperature. Geosci Model Dev 15(6):2653–2671

Careto JAM, Soares PMM, Cardoso RM et al (2022b) Added value of EURO-CORDEX high-resolution downscaling over the Iberian Peninsula revisited—part 1: precipitation. Geosci Model Dev 15(6):2635–2652. https://doi.org/10.5194/gmd-15-2635-2022

Ciarlo JM, Coppola E, Fantini A et al (2021) A new spatially distributed added value index for regional climate models: the EURO-CORDEX and the CORDEX-CORE highest resolution ensembles. Clim Dyn 57(5–6):1403–1424. https://doi.org/10.1007/s00382-020-05400-5

Coppola E, Raffaele F, Giorgi F et al (2021) Climate hazard indices projections based on CORDEX-CORE, CMIP5 and CMIP6 ensemble. Clim Dyn 57:1–91. https://doi.org/10.1007/s00382-021-05640-z

Cuadrat JM, Serrano-Notivoli R, Tejedor E, Saz MÁ, Prohom M, Cunillera J, Llabrés A, Trapero L, Pons M, López-Moreno JI, Copons R, Gascoin S, Luna Y, Rodríguez E, Ramos P, Amblar P, Soubeyroux J-M (2020) CLIMPY: Climate of the Pyrenees (1.0) [Data set]. Zenodo. https://doi.org/10.5281/zenodo.3611127

Dai A (2001) Global precipitation and thunderstorm frequencies. Part I: seasonal and interannual variations. J Clim 14(6):1092–1111. https://doi.org/10.1175/1520-0442(2001)014<1092:GPATFP>2.0.CO;2

Di A, Ramo L (2013) Potential for added value in temperature simulated by high-resolution nested RCMs in present climate and in the climate change signal. Clim Dyn. https://doi.org/10.1007/s00382-012-1384-2

Di Luca A, Argüeso D, Evans JP et al (2016) Quantifying the overall added value of dynamical downscaling and the contribution from different spatial scales. J Geophys Res 121(4):1575–1590. https://doi.org/10.1002/2015JD024009

Fantini A, Raffaele F, Torma C et al (2018) Assessment of multiple daily precipitation statistics in ERA-Interim driven Med-CORDEX and EURO-CORDEX experiments against high resolution observations. Clim Dyn 51(3):877–900. https://doi.org/10.1007/s00382-016-3453-4

Feser F (2006) Enhanced detectability of added value in limited-area model results separated into different spatial scales. Mon Weather Rev 134(8):2180–2190. https://doi.org/10.1175/MWR3183.1

Giorgi F, Jones C, Asrar G (2009) Addressing climate information needs at the regional level: the CORDEX framework. Organization (WMO) Bulletin 58(July):175–183. http://www.euro-cordex.net/uploads/media/Download_01.pdf

Gutowski JW, Giorgi F, Timbal B et al (2016) WCRP COordinated Regional Downscaling EXperiment (CORDEX): a diagnostic MIP for CMIP6. Geosci Model Dev 9(11):4087–4095. https://doi.org/10.5194/gmd-9-4087-2016

Isotta FA, Frei C, Weilguni V et al (2014) The climate of daily precipitation in the Alps: development and analysis of a high-resolution grid dataset from pan-Alpine rain-gauge data. Int J Climatol 34(5):1657–1675. https://doi.org/10.1002/joc.3794

Jacob D, Petersen J, Eggert B et al (2014) EURO-CORDEX: new high-resolution climate change projections for European impact research. Reg Environ Change 14(2):563–578. https://doi.org/10.1007/s10113-013-0499-2

Jacob D, Teichmann C, Sobolowski S et al (2020) Regional climate downscaling over Europe: perspectives from the EURO-CORDEX community. Reg Environ Change. https://doi.org/10.1007/s10113-020-01606-9

Jones CD, Hughes JK, Bellouin N et al (2011) The HadGEM2-ES implementation of CMIP5 centennial simulations. Geosci Model Dev 4(3):543–570. https://doi.org/10.5194/gmd-4-543-2011

Kämäräinen M, Hyvärinen O, Vajda A et al (2018) Estimates of present-day and future climatologies of freezing rain in Europe based on CORDEX regional climate models. J Geophys Res: Atmos 123(23):13291–13304. https://doi.org/10.1029/2018JD029131

Kotlarski S, Keuler K, Christensen OB et al (2014) Regional climate modeling on European scales: a joint standard evaluation of the EURO-CORDEX RCM ensemble. Geosci Model Dev 7(4):1297–1333. https://doi.org/10.5194/gmd-7-1297-2014

Kotlarski S, Lüthi D, Schär C (2015) The elevation dependency of 21st century European climate change: an RCM ensemble perspective. Int J Climatol 35(13):3902–3920. https://doi.org/10.1002/joc.4254

Lemus-Canovas M, Lopez-Bustins JA (2021) Assessing internal changes in the future structure of dry-hot compound events: the case of the Pyrenees. Nat Hazards Earth Syst Sci 21(6):1721–1738. https://doi.org/10.5194/nhess-21-1721-2021

Lemus-Canovas M, Lopez-Bustins JA, Trapero L et al (2019) Combining circulation weather types and daily precipitation modelling to derive climatic precipitation regions in the Pyrenees. Atmos Res 220(January):181–193. https://doi.org/10.1016/j.atmosres.2019.01.018

Liang XZ, Kunkel KE, Meehl GA et al (2008) Regional climate models downscaling analysis of general circulation models present climate biases propagation into future change projections. Geophys Res Lett 35(8):1–5. https://doi.org/10.1029/2007GL032849

McSweeney CF, Jones RG, Lee RW et al (2015) Selecting CMIP5 GCMs for downscaling over multiple regions. Clim Dyn 44(11–12):3237–3260. https://doi.org/10.1007/s00382-014-2418-8

Minder JR, Letcher TW, Skiles SMK (2016) An evaluation of high-resolution regional climate model simulations of snow cover and albedo over the rocky mountains, with implications for the simulated snow-albedo feedback. J Geophys Res 121(15):9069–9088. https://doi.org/10.1002/2016JD024995

Perkins SE, Pitman AJ, Holbrook NJ et al (2007) Evaluation of the AR4 climate models' simulated daily maximum temperature, minimum temperature, and precipitation over Australia using probability density functions. J Clim 20(17):4356–4376. https://doi.org/10.1175/JCLI4253.1

Prein AF, Gobiet A, Truhetz H et al (2016) Precipitation in the EURO-CORDEX 0.11o and 0.44o simulations: high resolution, high benefits? Clim Dyn 46(1-2):383–412. https://doi.org/10.1007/s00382-015-2589-y

Qiu L, Im ES, Hur J et al (2020) Added value of very high resolution climate simulations over South Korea using WRF modeling system. Clim Dyn 54(1–2):173–189. https://doi.org/10.1007/s00382-019-04992-x

Reder A, Raffa M, Montesarchio M et al (2020) Performance evaluation of regional climate model simulations at different spatial and temporal scales over the complex orography area of the Alpine region. Nat Hazards 102(1):151–177. https://doi.org/10.1007/s11069-020-03916-x

RiosEntenza A, Soares P, Trigo R et al (2014) Moisture recycling in the Iberian peninsula from a regional climate simulation: spatiotemporal analysis and impact on the precipitation regime. J Geophys Res: Atmos. https://doi.org/10.1002/2013JD021274

Rummukainen M (2016) Added value in regional climate modeling. Wiley Interdiscip Rev: Clim Change 7(1):145–159. https://doi.org/10.1002/wcc.378

Serrano-Notivoli R, Beguería S, Saz MÁ et al (2017) Spread: a high-resolution daily gridded precipitation dataset for Spain—an extreme events frequency and intensity overview. Earth Syst Sci Data 9(2):721–738. https://doi.org/10.20350/digitalCSIC/7393

Soares PM, Cardoso RM (2018) A simple method to assess the added value using high-resolution climate distributions: application to the EURO-CORDEX daily precipitation. Int J Climatol 38(3):1484–1498. https://doi.org/10.1002/joc.5261

Terzago S, von Hardenberg J, Palazzi E et al (2017) Snow water equivalent in the Alps as seen by gridded data sets, CMIP5 and CORDEX climate models. Cryosphere 11(4):1625–1645. https://doi.org/10.5194/tc-11-1625-2017

Torma C, Giorgi F, Coppola E (2015) Added value of regional climate modeling over areas characterized by complex terrain—precipitation over the Alps. AGU 175(4449):238. https://doi.org/10.1038/175238c0

van Meijgaard E, Crewell S (2005) Comparison of model predicted liquid water path with ground-based measurements during CLIWA-NET. Atmos Res 75(3):201–226. https://doi.org/10.1016/j.atmosres.2004.12.006

Vautard R, Kadygrov N, Iles C et al (2021) Evaluation of the large EURO-CORDEX regional climate model ensemble. J Geophys Res: Atmos 126(17):1–28. https://doi.org/10.1029/2019JD032344

Zappa G, Shaffrey LC, Hodges KI (2013) The ability of CMIP5 models to simulate North Atlantic extratropical cyclones. J Clim 26(15):5379–5396. https://doi.org/10.1175/JCLI-D-12-00501.1